Prediction Of Geospace Radiation Environment and Solar wind parameterS

Work Package 5
Low energy electrons model improvements to develop forecasting products

Deliverable D5.4
Trial version of forecast model for low energy electrons

N. Ganushkina, S. Dubyagin, M. Balikhin, S. Walker, T. Arber, P. Wintoft
February 28, 2018

Document Change Record

Issue	Date	Author	Details
v1	18.02.2018	N. Ganushkina	To be revised when forecasts are available
v2	18.09.2018	N. Ganushkina	Revised after External Reviewer comments and forecasts become available

Table of Contents

1. Introduction

The **Deliverable D5.4** entitled "Trial version of forecast model for low energy electrons" is the fourth Deliverable of the **WP5** "Low energy electrons model improvements to develop forecasting products". The fourth objective of this WP is to develop a trial version of forecast model for low energy electrons. During the work under the Deliverable **D5.4**, the main focus was set at the **Task 5.4** "Developing a trial version of forecast model for low energy electrons".

The low energy electrons model used here is the IMPTAM (Inner Magnetosphere Particle Transport and Acceleration Model) which is driven by (1) solar wind number density N_{SW}, (2) solar wind dynamic pressure P_{SW}, (3) solar wind velocity V_{SW}, (4) *IMF B_Y, B_Z,* and B_{IMF}, (5) *Dst* index, (6) *Kp* index, and (7) *AE* index. With forecasted driving parameter, the IMPTAM can predict the keV electron fluxes in the inner magnetosphere.

The forecasted solar wind and IMF parameters are now available again (started on April 23, 2018) at the University of Warwick. There was a break during the year 2018 with the latest dates available from 2018-01-19T12:17 until 2018-02-02T12:17. The present Deliverable D5.4 is now being revised due to re-appearance of that forecast. The forecasted geomagnetic indices were not provided by IRF-Lund at the moment of the end of the project (July 31, 2018). Currently, the predictions provided are only using measured solar wind and IMF parameters, not the predicted ones. Therefore, the *Kp* index is given for 3 hours ahead, the *Dst*-index for 1 hour ahead and the *AE*-index for 15 minutes ahead. Using such short-time forecasts does not provide any good for the IMPTAM as a forecasting model.

The completely re-organized IMPTAM is now running online as a near real-time version and forecast version. It uses the forecasted solar wind and IMF parameters when available but it does not use the IRF-Lund geomagnetic indices since they were not forecasted. Below, we demonstrate the general structure of the forecasting and nowcasting IMPTAM.

2. Brief description of IMPTAM

The IMPTAM (Inner Magnetosphere Particle Transport and Acceleration Model) [*Ganushkina et al.*, 2013, 2014, 2015] traces distributions of electrons in the drift approximation with arbitrary pitch angles from the plasma sheet to the inner L-shell regions with energies reaching up to hundreds of keVs in time-dependent magnetic and electric fields. We trace a distribution of particles in the drift, approximation, and we take into account the **ExB** drift, and magnetic drifts with bounce-average drift velocities. Relativistic effects for electrons are taken into account in the drift velocities.

To follow the evolution of the particle distribution function f and particle fluxes in the inner magnetosphere dependent on the position R, time t, energy E_{kin}, and pitch angle α, it is necessary to specify: (1) particle distribution at initial time at the model boundary; (2) magnetic and electric fields everywhere dependent on time; (3) drift velocities; (3) all sources and losses of particles. The changes in the distribution function f(R, φ, t, E_{kin}, α), where R and φ are the radial and azimuthal coordinates in the equatorial plane, respectively, are obtained by

solving the equation $\dfrac{df}{dt} = \dfrac{\partial f}{\partial t} \cdot V_\varphi + \dfrac{\partial f}{\partial t} V_R + sources - losses$, where V_φ and V_R are the azimuthal and radial components of the bounce-average drift velocity. The model boundary can be set in the plasma sheet at distances, depending on the scientific questions we are trying to answer, from 6.6 R_E to 10 R_E. Liouville's theorem is used to gain information of the entire distribution function by mapping the boundary conditions throughout the simulation domain, including loss process attenuation, through the time-varying magnetic and electric fields.

For the obtained distribution we apply radial diffusion which plays a significant role in electron energization. We solve the radial diffusion [*Schulz and Lanzerotti*, 1974] for the obtained distribution function. Kp-dependent radial diffusion coefficients D_{LL} for the magnetic field fluctuations are computed following *Brautigam and Albert* [2000]. Since diffusion by the magnetic field fluctuations at L > 3 dominates diffusion produced by electrostatic field fluctuations [*Shprits and Thorne*, 2004], we ignore the electrostatic component of the radial diffusion coefficient. At the next time step we repeat the order of calculation: first we solve transport with losses and then apply the diffusion.

Convective outflow, Coulomb collisions and loss to the atmosphere are taken into account. We assume strong pitch angle scattering at the distances where the ratio between the radius of the field line curvature in the equatorial current sheet R_c and the effective Larmor radius ρ varies between 6 and 10 [*Sergeev and Tsyganenko*, 1982; *Delcourt et al.*, 1996]. Electron precipitation to the atmosphere is calculated similarly to *Jordanova et al.* [2008] with a time scale of a quarter bounce period, and the loss cone corresponds to an altitude of 200 km. We take into account pitch angle diffusion due to wave-particle interactions by introducing the parameterizations of the electron lifetimes due to interactions with chorus and hiss waves by *Orlova and Shprits* [2014] and *Orlova et al.* [2014, 2016] with the activity-dependent plasmapause location by *Carpenter and Anderson* [1992].

IMPTAM can utilize any magnetic or electric field model. IMPTAM can take into account the self-consistency of the magnetic field by calculating the magnetic field produced by the model currents and feeding it back to the background magnetic field. At the same time, when using realistic model magnetic field such as Tsyganenko models which contain the prescribed ring and near-Earth tail currents, it is necessary to remove the model currents from the background magnetic field model and consider self-consistent calculations of the magnetic field. Since we study the electrons, their contribution to the ring current is no more than 10%, so their contribution to the distortion of the background magnetic field is small. Taking into account the electric field in a self-consistent way is of high importance when modeling the inner magnetosphere particles [*Fok et al.*, 2003; *Liemohn and Brandt*, 2005]. In our study, we focus on low-energy electrons and, therefore, neglect electron pressures in the total pressure as their effect is small/insignificant, so the chosen field models do not require any modifications for self-consistency effects. In addition to the large-scale fields, transient fields associated with the dipolarization process in the magnetotail during substorm onset were modeled [e.g., *Ganushkina et al.*, 2005] as an earthward propagating electromagnetic pulse of localized radial and longitudinal extent [*Li et al.*, 1998; *Sarris et al.*, 2002].

3. Driving parameters for IMPTAM

IMPTAM is driven by various solar wind, IMF and geomagnetic indices which are used as inputs for the different components of IMPTAM. We used Tsyganenko T96 magnetic field model [*Tsyganenko*, 1995] which uses the *Dst* index, P_{SW}, and *IMF* B_Y and B_Z as input parameters. The electric field was determined using V_{SW}, the IMF strength B_{IMF} and B_Y and B_Z (via IMF clock angle θ_{IMF}) being the *Boyle et al.* [1997] ionospheric potential Φ mapped to the magnetosphere.

We set the model boundary in the plasma sheet at 10 R_E and use the kappa electron distribution function. Parameters of the kappa distribution function are the plasma sheet number density N_{ps} and temperature T_{ps} given by the *Dubyagin et al.* [2016] empirical model, constructed at distances between 6 and 11 R_E based on THEMIS data. The N_{ps} is driven by the solar wind number density N_{sw} and southward IMF component B_S. The T_{ps} is dependent on solar wind velocity V_{sw} and the southward B_S and the northward B_N IMF components. $B_S = -$IMF B_Z, if IMF $B_Z < 0$ and $B_S = 0$, if IMF $B_Z \geq 0$; $B_N = 0$, if IMF $B_Z < 0$ and $B_N =$ IMF B_Z , if IMF $B_Z \geq 0$.

Figure 1 is an example of the IMPTAM behaviour with driving parameters taken from *Ganushkina et al.* [2018] as the comparison between the electron fluxes observed by GOES 13 MAGED instrument (panels (a), (d), and (g)) and modeled by IMPTAM (panels (b), (e), and (h)) for energies of 40, 75, and 150 keV and organized by the solar wind velocity and MLT. The size of the bins is 1 hour for MLT and 20km/s for Vsw. The data and the IMPTAM output were averaged inside each bin. Panels (c), (f), and (i) present the ratio between the modeled and observed fluxes in the logarithmic scale. The U-shaped peaks in the observed electron fluxes are located at 00-12 MLT and the fluxes increase with the increase of *Vsw* covering larger range of MLT. The modeled fluxes are rather close to the observed ones with ratio about one at 06-12 MLT. The main over-estimation is seen at around midnight but it is of about one order of magnitude. In general, the modeled fluxes are rather similarly organized with Vsw as the observed ones but the shift of peaks to midnight instead of dawn is present.

The parameterizations of the electron lifetimes due to interactions with chorus and hiss waves by *Orlova and Shprits* [2014] and *Orlova et al.* [2014, 2016] used to represent electron losses in IMPTAM depend on *Kp* index. *Kp* index is also the activity driver for the plasmapause location in *Carpenter and Anderson* [1992] used in IMPTAM.

Figure 2 presents another example from *Ganushkina et al.* [2017] of the modeled and observed electron fluxes binned by MLT (1 hour step) and *Kp* index (4 steps per 1 Kp value), and then averaged inside each bin, together with the ratio between them. The pattern how the observed electron fluxes depend on *Kp*-index along the geostationary orbit is rather similar to the one for *Vsw* (**Figure 1**) with the U-shaped peaks on the dawnside with fluxes increasing with *Kp* increase. The modeled fluxes are reasonably close to the observed fluxes at 06-18 MLT with the ratio much less than one order of magnitude.

Substorm-associated electromagnetic fields are taken into account in IMPTAM [*Ganushkina et al.*, 2013; 2014] in a similar form to the *Li et al.* [1998] and *Sarris et al.* [2002] model to represent an earthward-propagating electromagnetic pulse of localized radial and longitudinal extent. The pulse stops at 3.5 R_E. The magnetic field disturbance from this dipolarization process is obtained from
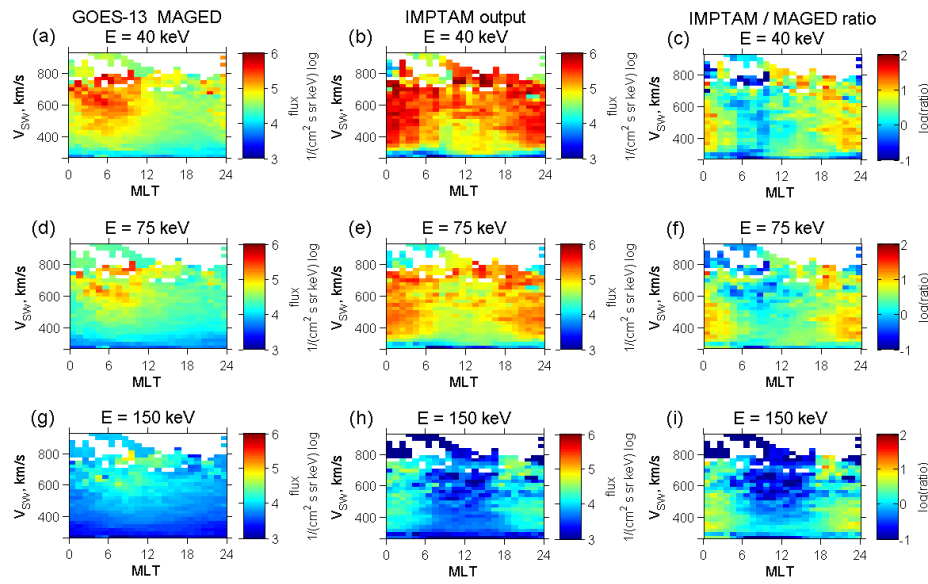
Figure 1. Flight-direction integrated differential electron fluxes [*Sillanpää et al.*, 2017] in logarithmic scale for the energies of 40, 75, and 150 keV computed from the GOES-13 MAGED data (panels (a), (d), and (g)) and modeled by the IMPTAM (panels (b), (e), and (h)) binned by MLT (1 hour step) and solar wind velocity Vsw (20 km/s step), and then averaged inside each bin, together with the ratio between them in logarithmic scale (panels (c), (f), and (i)).
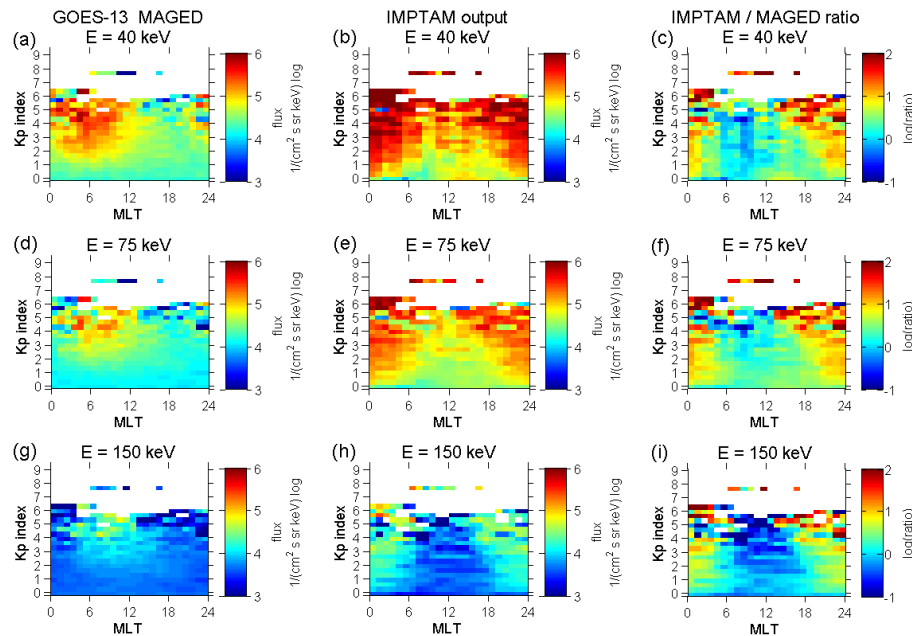

Figure 2. Similar to **Figure 1** but the observed and modeled electron fluxes are binned by MLT (1 hour step) and *Kp* index (4 steps per Kp value) and then averaged inside each bin.

Faraday's law. We launch a pulse at each substorm onset determined from the *AE* index and scaled the amplitude according the maximum values of the *AE*.

Thus, IMPTAM is driven by
    (1) Solar wind number density N_{SW},
    (2) Solar wind dynamic pressure P_{SW},
    (3) Solar wind velocity V_{SW},
    (4) IMF B_Y, B_Z, and B_{IMF}
    (5) *Dst* index,
    (6) *Kp* index,
    (7) *AE* index.

If these driving parameters can be forecasted, then used in IMPTAM they can drive IMPTAM to forecast keV electron fluxes in the inner magnetosphere.

4. Nowcast and Forecast IMPTAM architecture

IMPTAM for keV electrons has been run online in near-real time [*Ganushkina et al.*, 2015] since February 2013. The first nowcast version of IMPTAM was developed during the *SPACECAST project* (**http://fp7-spacecast.eu/**) and further applied to extreme space weather events during *SPACESTORM project* (**http://www.spacestorm.eu/**). The IMPTAM internal architecture is presented in **Figure 3**. There are 2 simulations going on, first is the real-time simulation and second is the forecast simulation. For the real-time simulator, the driving parameters (RealTime_DataSource) are obtained from the corresponding sources. Solar wind and IMF data as well as Kp index are obtained from from NOAA's Space Weather Prediction Center (http://services.swpc.noaa.gov/text/), Dst Index comes from the World Data Center for Geomagnetism, Kyoto University, Japan (wdc.kugi.kyoto-u.ac.jp/dst_realtime), AE is also taken from Kyoto University by special agreement with Dr. Nose.

    All the input parameters go to the Mongo database (installation instructions are openly available at https://docs.mongodb.com/manual/tutorial/install-mongodb-on-red-hat/). The real-time simulator downloads the input parameters from the database, runs the simulation and outputs the results. Second simulator, the forecast simulator, gets the output from the real-time simulator as files of 3D electron distribution functions electron_image_map f (r, lon, pitch_angle, mag_moment), where r is the radial distance, lon is the longitude, pitch_angle is the electron's pitch angle and mag_moment is the electron's magnetic moment. The header example looks as (was presented in details in the **Deliverable D5.3**):

```
<header
    step="480" INSIDE STEP
    timeRun="57600" TIME IN SECONDS
    time="1054224000"> UNIX TIME
     <data type="grid">
        <grid
        info="Rs, Re" RADIUS, ACTUALLY, L*, UNITLESS
        node="{1 30 3 9}"> 1-LINEAR GRID, 30-NUMBER OF INTERVALS IN R, 3-
RMIN, 9-RMAX
        <grid
                info="Longitude, deg" LONGITUDE, LONGITUDE=0 AT NOON
                node="{3 60}"/> FROM 0 TO 2PI, 60-NUMBER OF INTERVALS IN
LONGITUDE
```

```
    </grid>
    <data
        Type="grid">
        <grid
            info="B/Beq, #" USED FOR 2nd INVARIANT AND PITCH ANGLE, 1-
PA OF 90 DEG
            node="[1 1.04 1.09648 1.31826 1.58489 1.90546 2.29087 2.75423
3.31131 3.98107 4.7863 5.7544 6.91831 8.31764 10 12.0226 14.4544 17.378
20.893 25.1189 30.1995 36.3078 43.6516 52.4807 63.0957 75.8578]">
                <grid
                    info="MagMoment, keV/nT" MAGNETIC MOMENT, NOT
ENERGY
                    node="{2 45 0.002 6}"/> 2-LOG, 45-INTERVALS, 0.002-
MIN, 6-MAX
        </grid>
        <data
            type="unit"
            info="phaseden, f"/> MULTIPLY F BY ENERGY TO HAVE FLUX IN
1/CM2 S SR KEV
        </data>
    </data>
</header>
```

The Mongo database for forecasted IMPTAM driving parameters is filled in the same was as described for the real-time database but using different data sources. The solar wind and IMF parameters are taken from the University of Warwick (https://warwick.ac.uk/fac/sci/physics/research/cfsa/people/bennett/swift-data/results3/) and the geomagnetic indices are obtained from the NOAA's Space Weather Prediction Center and the World Data Center for Geomagnetism, Kyoto University, Japan and extrapolated for future moments using the values at the moment of modelling. As was mentioned in the Introduction, the forecasted geomagnetic indices were not provided by IRF-Lund at the moment of the end of the project (July 31, 2018). The predictions made by using only the measured solar wind and IMF parameters, not the predicted ones, do not provide any good for the IMPTAM as a forecasting model. The forecast simulator runs from the real time moment to the number of hours in the future whenever forecasted driving parameters are available.

Figure 4 contains the repetitions from **Figure 3** related to simulators and databases but it demonstrates how the output from the IMPTAM is made available for the outside users. We start with the Realtime data services description. "DataEngine" service is a special python script that send (HTTP/GET) request to defined public data service, extract data from response and insert/update specific data into database (MongoDb 3.6) collection. Data stored in MongoDB database collections:

"data collection kp" {time, [kp]}
"data collection magSph" {time, [Dst, AE]}
"data collection imf" {time, [IMF_BX, IMF_BY, IMF_BZ, IMF_B]}

"data collection solWind" {time, [NDEN, PRESSURE, VEL_X, VEL_Y, VEL_Z, VEL_B]}

Realtime IMPTAM simulator use those data. "DataEngine" services run periodically (every 20 min try to get data as close to realtime as possible).

Forecast data services are similar: "DataEngine" service requests forecast data (solar wind, IMF and indices) from the forecast services. Forecast IMPTAM simulator use those forecast data to run simulation for future request interval (typically 24 hours). Forecast IMPTAM simulator runs periodically (typically 24h) to produce forecast with new parameters. Initial distributions of particles (electrons and ions) are loaded from images created by realtime IMPTAM simulation.

Web service has been developed to present and deliver IMPTAM simulation results. Web service build using Node.Js www server connected with MongoDB where IMPTAM simulation results are stored. IMPTAM realtime and forecast service currently hosted at http://citrine.engin.umich.edu. The web server presents IMPTAM simulation results in client's web browser (http://citrine.engin.umich.edu/IMPTAM) and return data in JSON format on [HTTP/GET] request (REST_API): for example,
http://address/imptam/api/result/realtime/"dataname"?timeStart=&timeEnd=
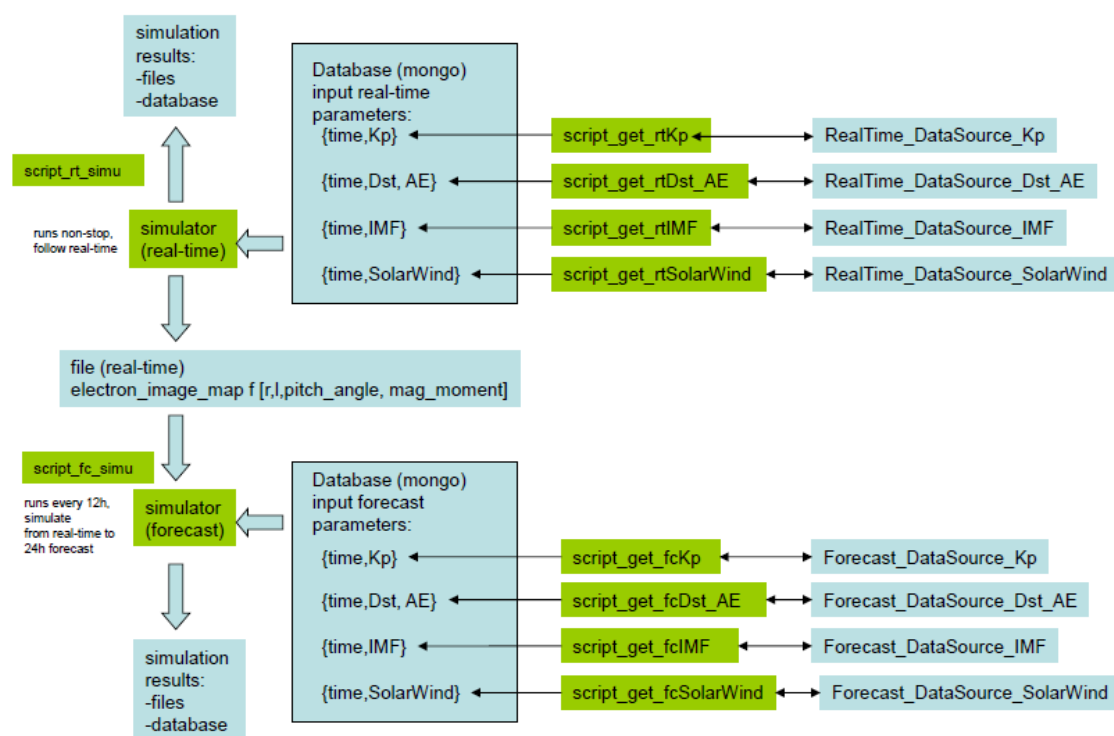

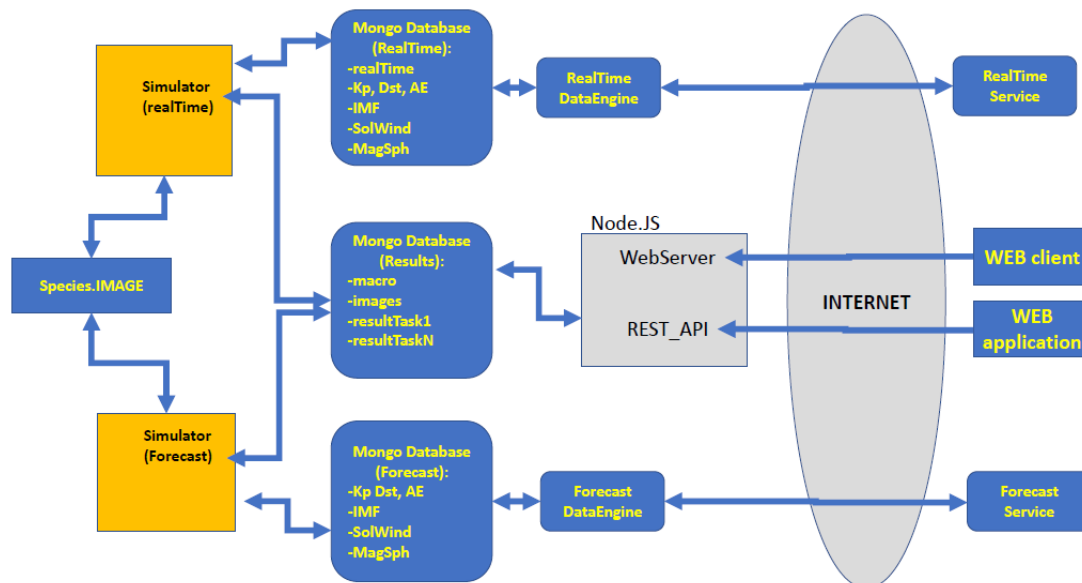
Figure 3. IMPTAM internal architecture

Figure 4. IMPTAM output availability.

Parameter data_name is a name of data (simulation results or collected simulation parameters) collection stored in database. Any data collection marked as public available in database can be requested via that REST_API. Optional parameters timeStart and timeEnd are used to specify requested data time interval. The timeStart and timeEnd is UT time in ISO8601 format. For example, the request:

http://citrine.engin.umich.edu/api/data/dataFluxGoes?timeStart=2018-02-11T16:30:00Z&timeEnd=2018-02-12T16:30:00

returns all data stored in collection named "dataFluxGoes" (electron and proton fluxes at GOES 15 satellite orbit) for UT time interval from 2018-02-11T16:30:00Z to 2018-02-12T16:30:00. The database contains electron and proton fluxes along the defined satellites trajectories, radial profiles, equatorial maps, e.g., 1D, 2D, 3D and 4D data tables.

5. Forecasted IMF and solar wind parameters as inputs to IMPTAM

As a result of the Task 2.7 "Run real-time test of predicted L1 variables based on coupled AWSoM/SWIFT codes in WP2 "Propagation of the Solar Wind from the Sun to L1", the forecasted solar wind and IMF parameters are now available at the University of Warwick at

https://warwick.ac.uk/fac/sci/physics/research/cfsa/people/bennett/swift-data/results3/

The available data are presented as .json files with the following structure:

Satellite	"Earth"
end_date	"2017-12-07T12:08"
Arrays	
Temperature_ion	{...}

Energy_electron	{...}
Time	{...}
Y_Position	{...}
Z_Position	{...}
Temperature_electron	{...}
Energy_ion	{...}
Unix time	{...}
Pressure	{...}
Pressure_ion	{...}
Rho	{...}
Bx	{...}
By	{...}
Bz	{...}
Vx	{...}
X_Position	{...}
Pressure_electron	{...}
Cs	{...}
Vy	{...}
Vz	{...}
co-ordinates	"Cartesian"
swift_version	"0.1.4"
start_date	"2017-11-23T12:04"
output_version	2
magnetogram_date	"2017-12-03T12:03"
co-ordinate system	"GSM"
swift_run_date	"Sat Nov 25 05:01:17 2017"
swift_commit_id	"v0.1.4-616-gdb0248c-dirty"

For IMPTAM input parameters we use

(1) Solar wind number density N_{SW}, computed as

N_{SW}[cm^-3] = Rho[kg/m^3]*4.9823E20 (coefficient takes into account 5% of Helium;

(2) use three components of solar wind velocity in m/s units and compute the total speed V_{sw} from them

(3) Solar wind dynamic pressure P_{SW}, computed as

P_{SW}[nPa] = Rho[kg/m^3] * V_{sw}[m/s]^2* 1.E9

(4) three components of IMF in T units, transform them in nT units and compute the total field B_{IMF} from them. *IMF B_Y, B_Z, and B_{IMF}.*
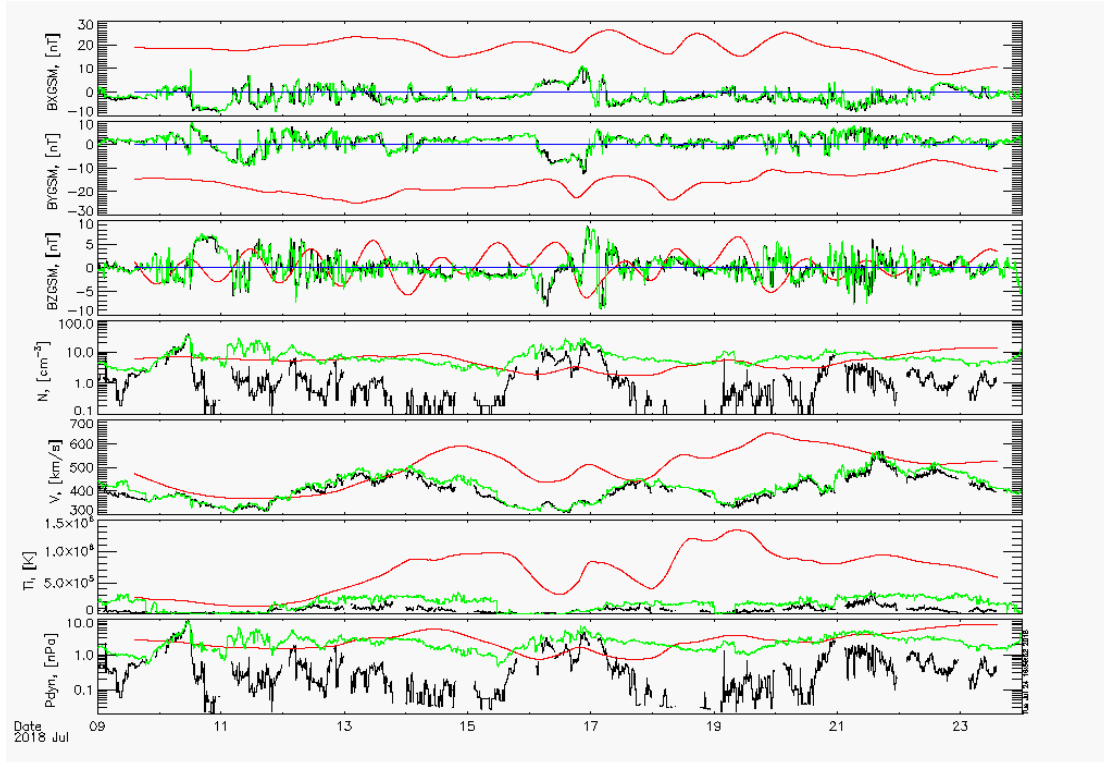
Figure 5. Solar wind and IMF parameters observed (black lines) at ACE and at DSCOVR (green lines) and modelled (red lines) by AWSoM/SWIFT for the time interval from July 9th, 2018, 00 UT until July 23d, 2018.

One example of the solar wind and IMF parameters observed (black lines) at ACE and at DSCOVR (green lines) and modelled (red lines) by AWSoM/SWIFT for the time interval from July 9th, 2018, 00 UT until July 23d, 2018, is presented in **Figure 5** for comparison. First three panels show the three components of the IMF, next is for the solar wind number density, then the solar wind speed is presented and two bottom panels demonstrate the behaviour of the ion temperature and the solar wind dynamic pressure. It can be seen that the forecasted parameters miss almost all of the smaller-scale variations seen in the observed parameters. At the same time, these are the only available forecasted solar wind and IMF parameters which can be used an input to the IMPTAM.

6. Forecasted Kp, Dst and AE indices as inputs to IMPTAM

As a result of Tasks 3.4 "Develop further existing Kp and Dst models", Task 3.5 "Develop new AE forecast models" and 3.6 "Implement models for real-time operation" of WP3 "Forecast of the evolution of geomagnetic indices" and Task 7.1 "Implementation of models for geomagnetic indices and electron flux forecasts at USFD" in WP7 "Fusion of forecasting tools", IRF-Lund is now providing the predictions of *Kp, Dst* and *AE* indices. **Currently the predictions provided are only using measured solar wind, not predicted solar wind.**

For example, at the moment in time UT on Wed Feb 7 09:00:50 UTC 2018, accessing the rest service with
http://lund.irf.se/progress/rest/datasets/irfkp2017/latest?limit=10
results in getting

ts,kp
2018-02-06 09:00:00+00:00,1.98240619897842
2018-02-06 12:00:00+00:00,1.08166609704494
2018-02-06 15:00:00+00:00,1.05537723004818
2018-02-06 18:00:00+00:00,1.14828304946423
2018-02-06 21:00:00+00:00,1.29495093226433
2018-02-07 00:00:00+00:00,0.90431709587574
2018-02-07 03:00:00+00:00,0.595133766531944
2018-02-07 06:00:00+00:00,0.879624143242836
2018-02-07 09:00:00+00:00,0.944028943777084
2018-02-07 12:00:00+00:00,1.16593627631664

For the predicted values in the table above the timestamps indicate the start of the 3-hour interval. So, the last *Kp* prediction is valid for the 12-15UT interval. Generally, the last two values will change as new predictions are generated every minute.

The same is true for *Dst*, but the interval is 1 hour and the lead time is also shorter, http://lund.irf.se/progress/rest/datasets/irfdst2017/latest?limit=10

ts,dst
2018-02-07 01:00:00+00:00,-9.97956120967865
2018-02-07 02:00:00+00:00,-8.8495814204216
2018-02-07 03:00:00+00:00,-6.6657692193985
2018-02-07 04:00:00+00:00,-6.25508707761765
2018-02-07 05:00:00+00:00,-6.16576093435287
2018-02-07 06:00:00+00:00,-5.47864067554474
2018-02-07 07:00:00+00:00,-5.08679407835007
2018-02-07 08:00:00+00:00,-4.41077333688736
2018-02-07 09:00:00+00:00,-4.10982251167297
2018-02-07 10:00:00+00:00,-3.25984817743301

Thus, latest prediction is valid for 10-11UT.

Finally, AE, AL, and AU are available at http://lund.irf.se/progress/rest/datasets/irfae2017/latest?limit=10

ts,ae,al,au
2018-02-07 09:20:00+00:00,67.1063461303711,-32.578670501709,29.865442276001
2018-02-07 09:25:00+00:00,65.0807800292969,-30.0797252655029,29.344217300415
2018-02-07 09:30:00+00:00,62.6665382385254,-29.3200340270996,28.5473880767822
2018-02-07 09:35:00+00:00,63.1102714538574,-31.5656623840332,29.0033988952637
2018-02-07 09:40:00+00:00,62.426929473877,-32.9503974914551,29.590690612793
2018-02-07 09:45:00+00:00,62.1464958190918,-33.9130210876465,29.9237594604492
2018-02-07 09:50:00+00:00,61.8609924316406,-36.9930000305176,30.909387588501
2018-02-07 09:55:00+00:00,67.7665634155273,-46.6880531311035,34.1267509460449

2018-02-07 10:00:00+00:00,71.0041427612305,-
51.7344131469727,34.2435455322266
2018-02-07 10:05:00+00:00,79.3798217773438,-
56.9845733642578,37.7617454528809

The table above was accessed at 09:12:06 UT. The AE predictions are given with 5-minute resolution, therefore, the last prediction covers the 10:05-10:10UT interval.

The forecasted geomagnetic indices were not provided by IRF-Lund at the moment of the end of the project (July 31, 2018). Currently, the predictions provided are only using measured solar wind and IMF parameters, not the predicted ones. Therefore, the *Kp* index is given for 3 hours ahead, the *Dst*-index for 1 hour ahead and the *AE*-index for 15 minutes ahead. Using such short-time forecasts does not provide any good for the IMPTAM as a forecasting model.

7. Demonstration of real-time version of the model for low energy electrons
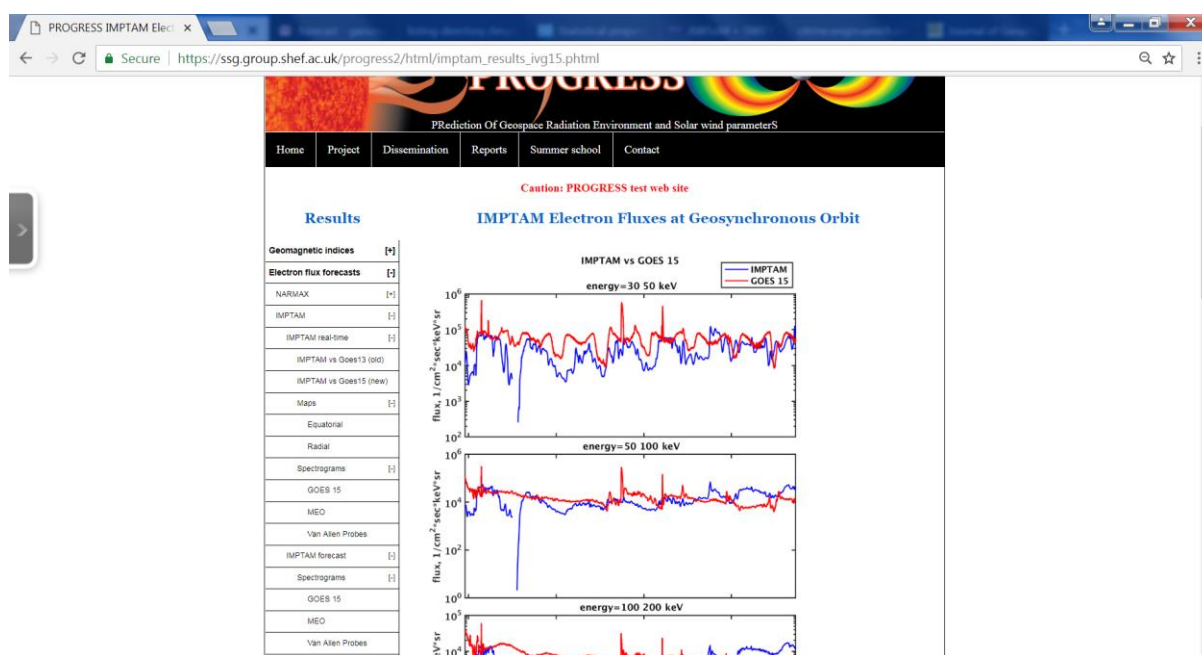

Figure 6. PROGRESS webpage at the University of Sheffield with demonstration of IMPTAM real-time features.

Figure 6 is for the demonstration of IMPTAM real-time features shown on the PROGRESS webpage at the University of Sheffield. IMPTAM real-time (**IMPTAM vs Goes 15 (new)**) includes the direct comparison with GOES 15 electron fluxes for 30-50, 50-100 and 100-200 keV energies (https://ssg.group.shef.ac.uk/progress2/html/imptam_results_ivg15.phtml) shown in **Figure 6** for the 3 days of August 2018. The current image taken on September 18, 2018 is presented at **Figure 7** with the time covered from July 31 to September 18.
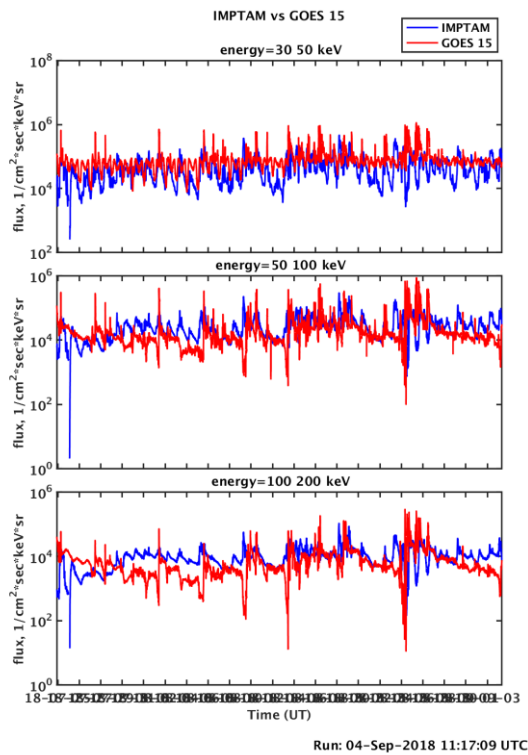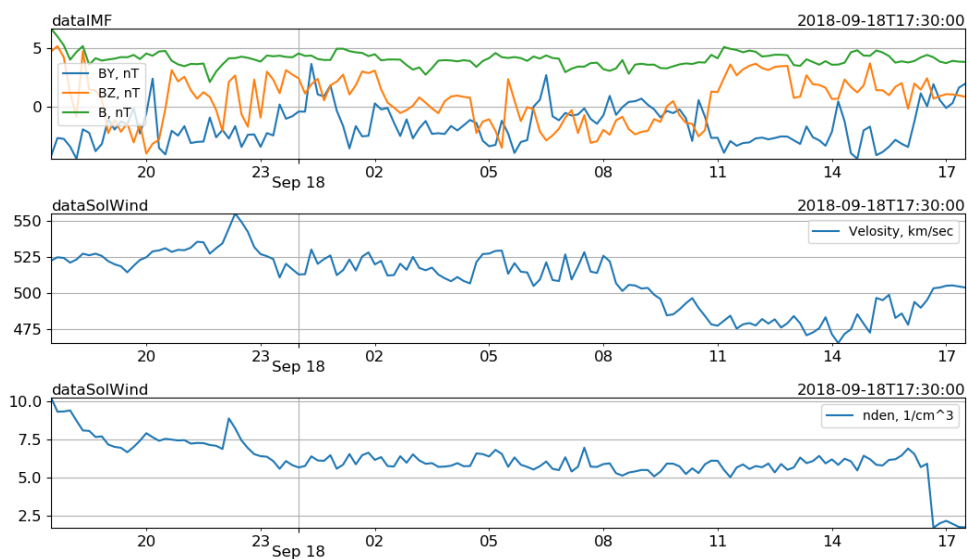
Figure 7. Direct comparison of IMPTAM results with GOES 15 electron fluxes for 30-50, 50-100 and 100-200 keV energies with the time covered from July 31 to September 18, 2018.

For the time moment when this text is being written (September 18, 2018), the driving parameters (http://citrine.engin.umich.edu/imptam/realtime/param) are presented in **Figure 8**.
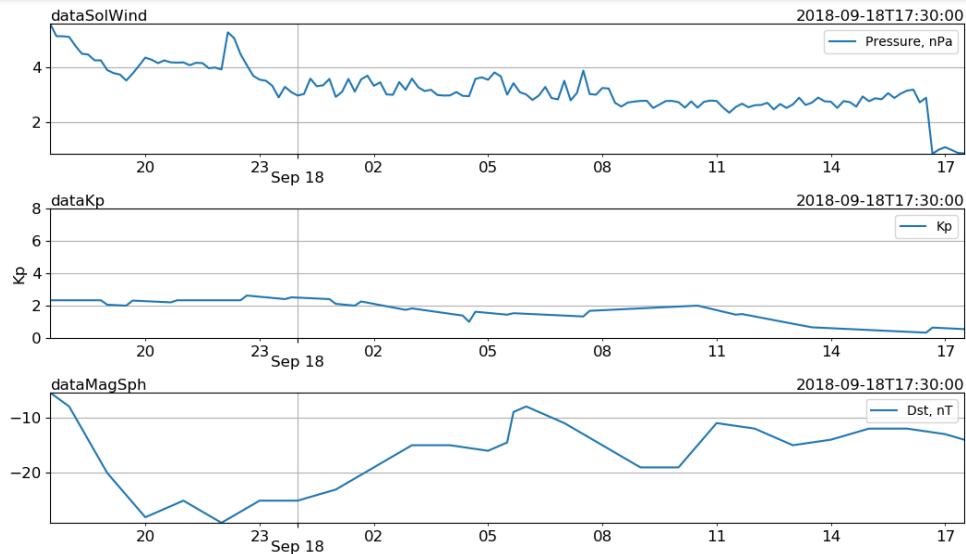
Figure 8. IMPTAM driving parameters.

The IMPTAM results called **Maps** (**Figure 9**) are presented as equatorial maps (**Equatorial**) of electron fluxes for 1-10, 10-50, 50-100 and 100-200 keV energies (https://ssg.group.shef.ac.uk/progress2/html/imptam_results_maps.phtml) and energy-radial distance spectrograms (**Radial**) for a current time moment at 0, 6, 12 and 18 MLT (https://ssg.group.shef.ac.uk/progress2/html/imptam_results_radial.phtml).
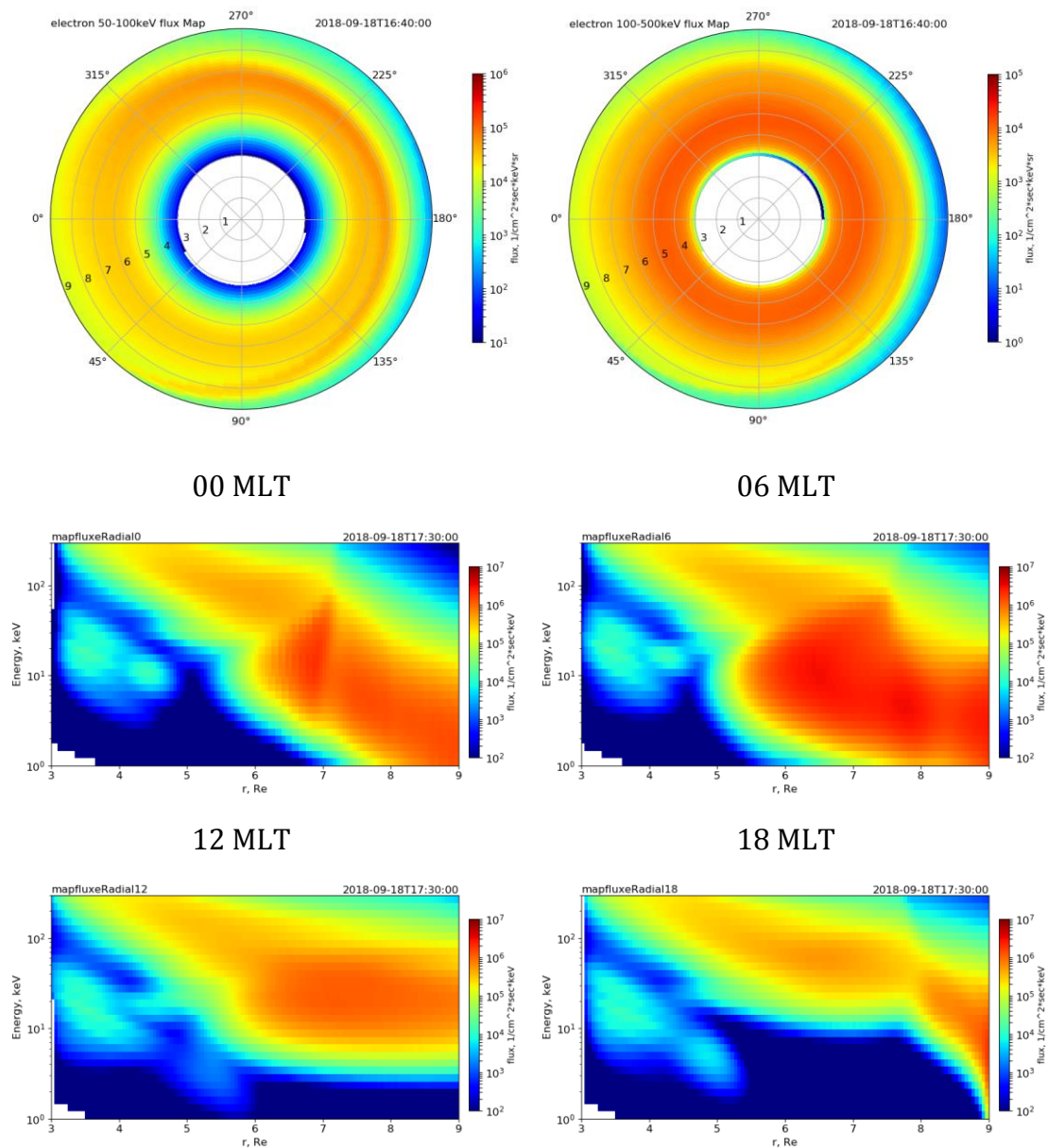
IMPTAM Real time equatorial maps
1-10 keV   10-50 keV

50-100 keV   100-500 keV
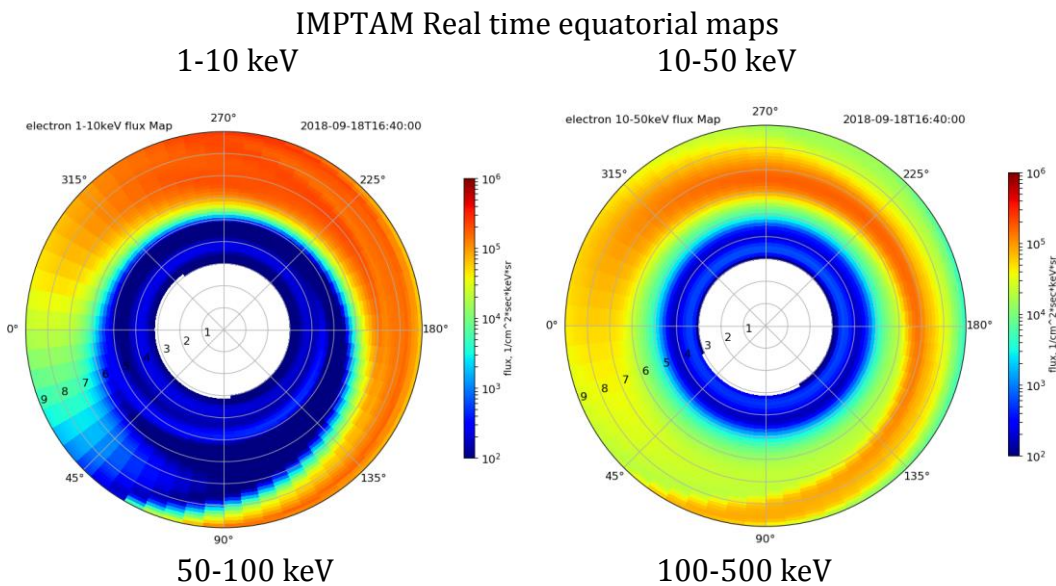
Figure 9. Equatorial and radial maps of electron fluxes for 1-10, 10-50, 50-100 and 100-200 keV energies.

The IMPTAM results called **Spectrograms** show the energy-time spectrograms along GOES 15
 (https://ssg.group.shef.ac.uk/progress2/html/imptam_results_spec_g15.phtml),
Galileo (MEO)
(https://ssg.group.shef.ac.uk/progress2/html/imptam_results_spec_meo.phtml)
and Van Allen Probes
 (https://ssg.group.shef.ac.uk/progress2/html/imptam_results_spec_vap.phtml)
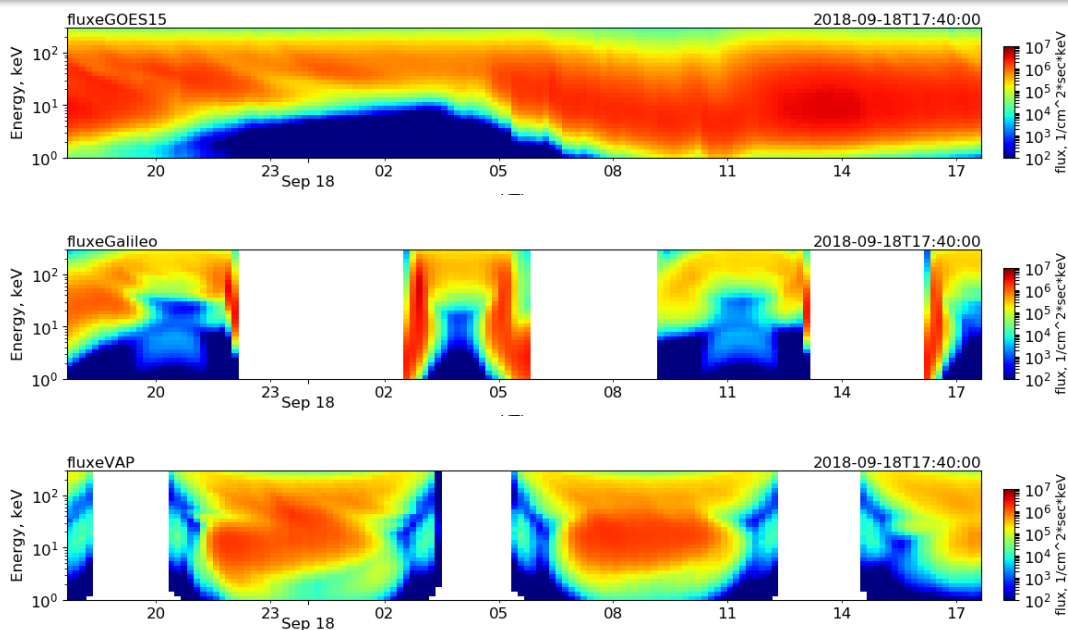orbits (**Figure 10**) in real time.

Figure 10. Energy-time spectrograms along GOES 15 (top panel), Galileo (MEO) (middle panel) and Van Allen Probes (bottom panel) orbits in real time.

All the data are available and can be taken following the instructions below:

IMPTAM realtime parameters

get: http://address/imptam/api/param/realtime/"dataname"?timeStart=&timeEnd=

timeStart and timeEnd are optional parameters can be given YYYY-MM-DD or YYYY-MM-DDTHH:MM:SSZ e.g.: timeStart=2018-07-18 timeEnd=2018-07-18T00:00:00Z

Name	Info
goes	{"comp":[{"info":"P1 flux, 1/cm^2*sec*keV*sr"},{"info":"P2 flux, 1/cm^2*sec*keV*sr"},{"info":"P3 flux, 1/cm^2*sec*keV*sr"},{"info":"P4 flux, 1/cm^2*sec*keV*sr"},{"info":"P5 flux, 1/cm^2*sec*keV*sr"},{"info":"E1 flux, 1/cm^2*sec*keV*sr"},{"info":"E2 flux, 1/cm^2*sec*keV*sr"},{"info":"E3 flux, 1/cm^2*sec*keV*sr"},{"info":"E4 flux, 1/cm^2*sec*keV*sr"},{"info":"E5 flux, 1/cm^2*sec*keV*sr"}]}
imf	{"comp":[{"info":"BX, nT"},{"info":"BY, nT"},{"info":"BZ, nT"},{"info":"B, nT"}]}
kp	{"info":"Kp"}
ms	{"comp":[{"info":"Dst, nT"},{"info":"Ae, nT"}]}
sw	{"comp":[{"info":"nden, 1/cm^3"},{"info":"Pressure, nPa"},{"info":"VelosityX, km/sec"},{"info":"VelosityY, km/sec"},{"info":"VelosityZ, km/sec"},{"info":"Velosity, km/sec"}]}

IMPTAM realtime result

get: http://address/imptam/api/result/realtime/"dataname"?timeStart=&timeEnd=

timeStart and timeEnd are optional parameters can be given YYYY-MM-DD or YYYY-MM-DDTHH:MM:SSZ e.g.: timeStart=2018-07-18 timeEnd=2018-07-18T00:00:00Z

Name	Info
dataFluxGoes	{"comp":[{"info":"P1 flux, 1/cm^2*sec*keV*sr"},{"info":"P2 flux, 1/cm^2*sec*keV*sr"},{"info":"P3 flux, 1/cm^2*sec*keV*sr"},{"info":"P4 flux, 1/cm^2*sec*keV*sr"},{"info":"P5 flux, 1/cm^2*sec*keV*sr"},{"info":"E1 flux, 1/cm^2*sec*keV*sr"},{"info":"E2 flux, 1/cm^2*sec*keV*sr"},{"info":"E3 flux, 1/cm^2*sec*keV*sr"},{"info":"E4 flux, 1/cm^2*sec*keV*sr"},{"info":"E5 flux, 1/cm^2*sec*keV*sr"}]}
dataIMF	{"comp":[{"info":"BX, nT"},{"info":"BY, nT"},{"info":"BZ, nT"},{"info":"B, nT"}]}
dataKp	{"info":"Kp"}
dataMagSph	{"comp":[{"info":"Dst, nT"},{"info":"Ae, nT"}]}
dataSolWind	{"comp":[{"info":"nden, 1/cm^3"},{"info":"Pressure, nPa"},{"info":"VelosityX, km/sec"},{"info":"VelosityY, km/sec"},{"info":"VelosityZ, km/sec"},{"info":"Velosity, km/sec"}]}
fluxeGOES15	{"data":{"info":"flux, 1/cm^2*sec*keV"},"grid":{"info":"Energy, keV","node":{"intrvNum":30,"scl":2,"valMax":300,"valMin":1}}}
fluxeGalileo	{"data":{"info":"flux, 1/cm^2*sec*keV"},"grid":{"info":"Energy, keV","node":{"intrvNum":30,"scl":2,"valMax":300,"valMin":1}}}
fluxeVAP	{"data":{"info":"flux, 1/cm^2*sec*keV"},"grid":{"info":"Energy, keV","node":{"intrvNum":30,"scl":2,"valMax":300,"valMin":1}}}
fluxpGOES15	{"data":{"info":"flux, 1/cm^2*sec*keV"},"grid":{"info":"Energy, keV","node":{"intrvNum":30,"scl":2,"valMax":300,"valMin":1}}}
fluxpGalileo	{"data":{"info":"flux, 1/cm^2*sec*keV"},"grid":{"info":"Energy, keV","node":{"intrvNum":30,"scl":2,"valMax":300,"valMin":1}}}
fluxpVAP	{"data":{"info":"flux, 1/cm^2*sec*keV"},"grid":{"info":"Energy, keV","node":{"intrvNum":30,"scl":2,"valMax":300,"valMin":1}}}
locationGOES15	{"comp":[{"info":"x, Re"},{"info":"y, Re"},{"info":"z, Re"}]}
locationGalileo	{"comp":[{"info":"x, Re"},{"info":"y, Re"},{"info":"z, Re"}]}
locationVAP	{"comp":[{"info":"x, Re"},{"info":"y, Re"},{"info":"z, Re"}]}
mcGOES15	{"comp":[{"info":"Rs"},{"info":"Lon, rad"},{"info":"B/Beq"},{"info":"B, nT"}]}
mcGalileo	{"comp":[{"info":"Rs"},{"info":"Lon, rad"},{"info":"B/Beq"},{"info":"B, nT"}]}

Name	Info
mcVAP	{"comp":[{"info":"Rs"},{"info":"Lon, rad"},{"info":"B/Beq"},{"info":"B, nT"}]}
pdfeGOES15	{"data":{"comp":[{"info":"flux, 1/cm^2*sec*keV*sr"}],"mask":"0x00000020"},"label":[" energy={30 50} keV"," energy={50 100} keV"," energy={100 200} keV"," energy={200 350} keV"," energy={350 600} keV"],"num":5}
pdfpGOES15	{"data":{"comp":[{"info":"flux, 1/cm^2*sec*keV*sr"}],"mask":"0x00000020"},"label":[" energy={80 110} keV"," energy={110 170} keV"," energy={170 250} keV"," energy={250 350} keV"," energy={350 800} keV"],"num":5}

8. Demonstration of trial version of forecast model for low energy electrons
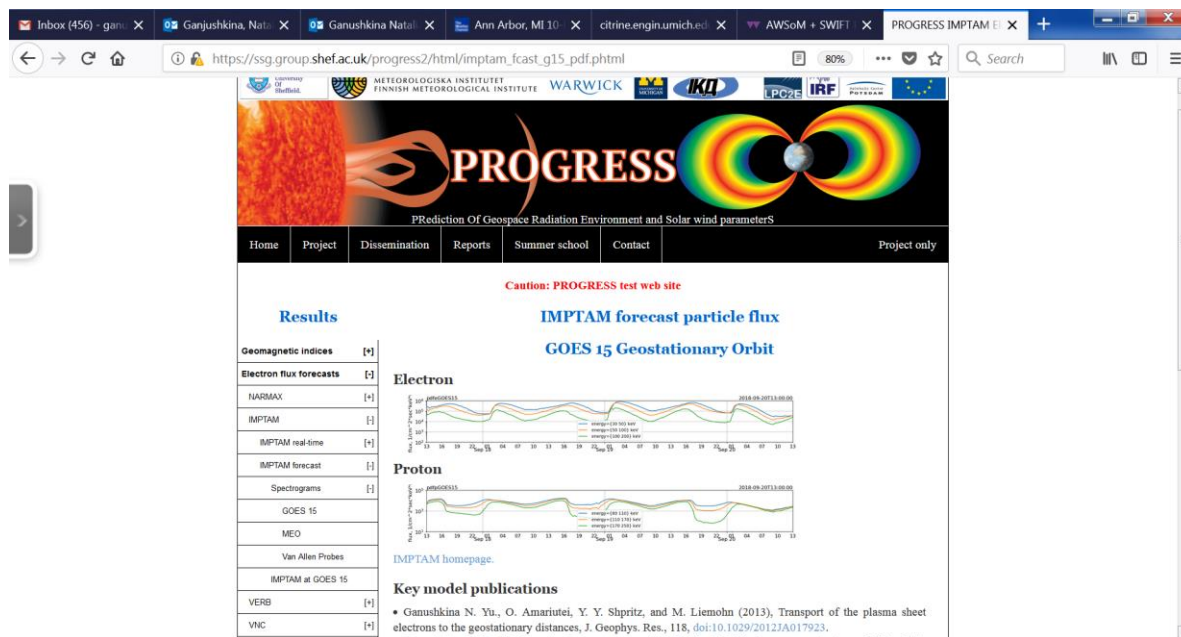

Figure 12. PROGRESS webpage at the University of Sheffield with demonstration of IMPTAM forecast features.

Figure 12 is for the demonstration of IMPTAM forecast features shown on the PROGRESS webpage at the University of Sheffield. At the moment of writing this text, the IMPTAM forecast was plotted for the period **from September 17, 2018, 1300 UT until September 20, 2018, 1300 UT**. The IMPTAM driving parameters (http://citrine.engin.umich.edu/imptam/forecast/param) are presented at **Figure 13** for this period. The IMPTAM results called **Spectrograms** show the energy-time spectrograms along GOES 15

(https://ssg.group.shef.ac.uk/progress2/html/imptam_fcast_g15.phtml), Galileo (MEO)
(https://ssg.group.shef.ac.uk/progress2/html/imptam_fcast_meo.phtml)
and Van Allen Probes
 (https://ssg.group.shef.ac.uk/progress2/html/imptam_fcast_vap.phtml)   orbits
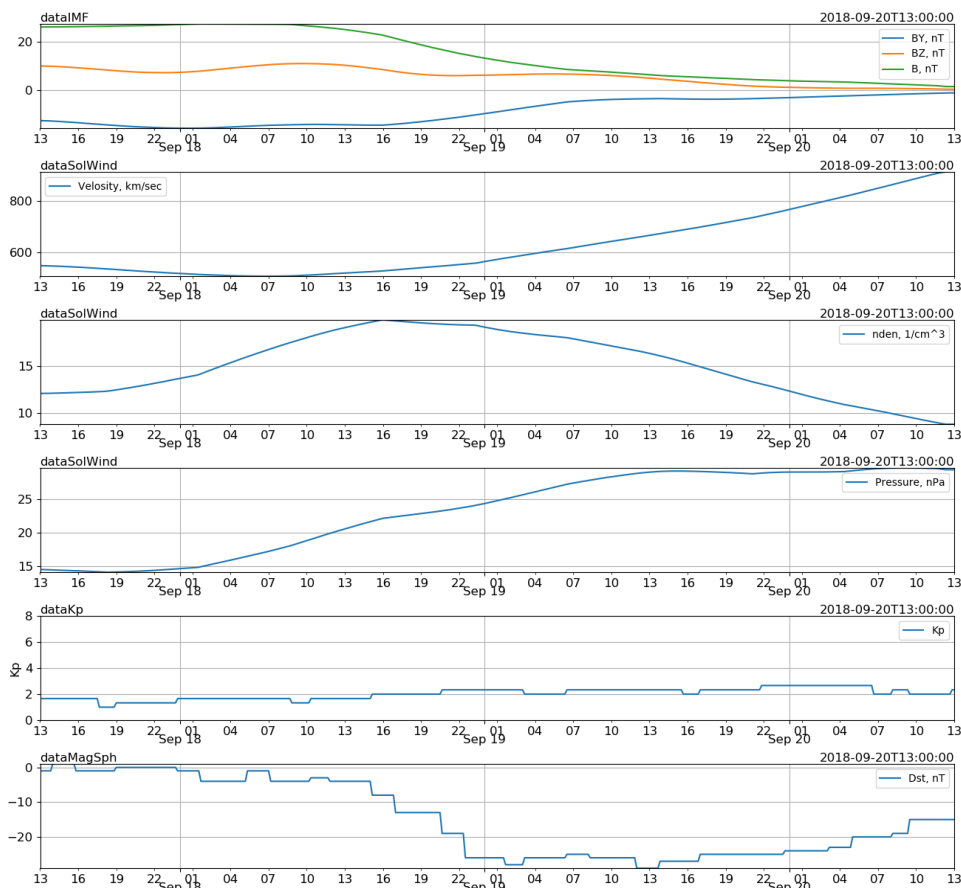(**Figure 14**).

Figure 13. IMPTAM driving parameters for the forecasted period from September 17, 2018, 1300 UT until September 20, 2018, 1300 UT.
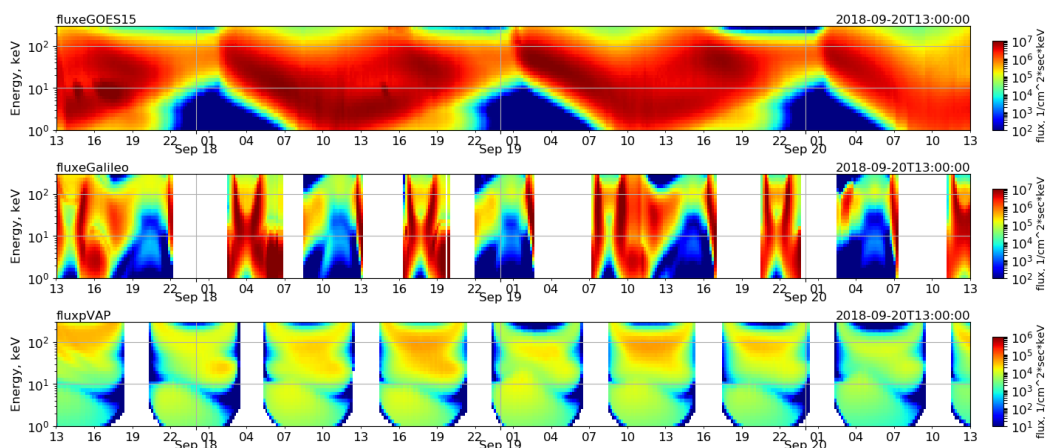

Figure 14. Forecasted energy-time spectrograms along GOES 15 (top panel), Galileo (MEO) (middle panel) and Van Allen Probes (bottom panel) orbits for the period from September 17, 2018, 1300 UT until September 20, 2018, 1300 UT.

IMPTAM forecast (**IMPTAM at Goes 15**) includes the IMPTAM output along GOES 15 orbit electron fluxes for 30-50, 50-100 and 100-200 keV energies and proton fluxes for 80-110, 110-170 and 170-250 keV energies (https://ssg.group.shef.ac.uk/progress2/html/imptam_fcast_g15_pdf.phtml) shown in **Figure 12**.

All the data are available and can be taken following the instructions below:

IMPTAM forecast parameters

get: http://address/imptam/api/param/forecast/"dataname"?timeStart=&timeEnd=

timeStart and timeEnd are optional parameters can be given YYYY-MM-DD or YYYY-MM-DDTHH:MM:SSZ e.g.: timeStart=2018-07-18 timeEnd=2018-07-18T00:00:00Z

Name	Info
imf	{"comp":[{"info":"BX, nT"},{"info":"BY, nT"},{"info":"BZ, nT"},{"info":"B, nT"}]}
sw	{"comp":[{"info":"nden, 1/cm^3"},{"info":"Pressure, nPa"},{"info":"VelosityX, km/sec"},{"info":"VelosityY, km/sec"},{"info":"VelosityZ, km/sec"},{"info":"Velosity, km/sec"}]}

IMPTAM forecast result

get: http://address/imptam/api/result/forecast/"dataname"?timeStart=&timeEnd=

timeStart and timeEnd are optional parameters can be given YYYY-MM-DD or YYYY-MM-DDTHH:MM:SSZ e.g.: timeStart=2018-07-18 timeEnd=2018-07-18T00:00:00Z

Name	Info
dataIMF	{"comp":[{"info":"BX, nT"},{"info":"BY, nT"},{"info":"BZ, nT"},{"info":"B, nT"}]}
dataKp	{"info":"Kp"}
dataMagSph	{"comp":[{"info":"Dst, nT"},{"info":"Ae, nT"}]}
dataSolWind	{"comp":[{"info":"nden, 1/cm^3"},{"info":"Pressure, nPa"},{"info":"VelosityX, km/sec"},{"info":"VelosityY, km/sec"},{"info":"VelosityZ, km/sec"},{"info":"Velosity, km/sec"}]}
fluxeGOES15	{"data":{"info":"flux, 1/cm^2*sec*keV"},"grid":{"info":"Energy, keV","node":{"intrvNum":30,"scl":2,"valMax":300,"valMin":1}}}
fluxeGalileo	{"data":{"info":"flux, 1/cm^2*sec*keV"},"grid":{"info":"Energy, keV","node":{"intrvNum":30,"scl":2,"valMax":300,"valMin":1}}}
fluxeVAP	{"data":{"info":"flux, 1/cm^2*sec*keV"},"grid":{"info":"Energy,

Name	Info
	keV","node":{"intrvNum":30,"scl":2,"valMax":300,"valMin":1}}}
fluxpGOES15	{"data":{"info":"flux, 1/cm^2*sec*keV"},"grid":{"info":"Energy, keV","node":{"intrvNum":30,"scl":2,"valMax":300,"valMin":1}}}
fluxpGalileo	{"data":{"info":"flux, 1/cm^2*sec*keV"},"grid":{"info":"Energy, keV","node":{"intrvNum":30,"scl":2,"valMax":300,"valMin":1}}}
fluxpVAP	{"data":{"info":"flux, 1/cm^2*sec*keV"},"grid":{"info":"Energy, keV","node":{"intrvNum":30,"scl":2,"valMax":300,"valMin":1}}}
locationGOES15	{"comp":[{"info":"x, Re"},{"info":"y, Re"},{"info":"z, Re"}]}
locationGalileo	{"comp":[{"info":"x, Re"},{"info":"y, Re"},{"info":"z, Re"}]}
locationVAP	{"comp":[{"info":"x, Re"},{"info":"y, Re"},{"info":"z, Re"}]}
mcGOES15	{"comp":[{"info":"Rs"},{"info":"Lon, rad"},{"info":"B/Beq"},{"info":"B, nT"}]}
mcGalileo	{"comp":[{"info":"Rs"},{"info":"Lon, rad"},{"info":"B/Beq"},{"info":"B, nT"}]}
mcVAP	{"comp":[{"info":"Rs"},{"info":"Lon, rad"},{"info":"B/Beq"},{"info":"B, nT"}]}
pdfeGOES15	{"data":{"comp":[{"info":"flux, 1/cm^2*sec*keV*sr"}],"mask":"0x00000020"},"label":[" energy={30 50} keV"," energy={50 100} keV"," energy={100 200} keV"," energy={200 350} keV"," energy={350 600} keV"],"num":5}
pdfpGOES15	{"data":{"comp":[{"info":"flux, 1/cm^2*sec*keV*sr"}],"mask":"0x00000020"},"label":[" energy={80 110} keV"," energy={110 170} keV"," energy={170 250} keV"," energy={250 350} keV"," energy={350 800} keV"],"num":5}

9. Conclusions

The low energy electrons model IMPTAM is driven by (1) solar wind number density N_{SW}, (2) solar wind dynamic pressure P_{SW}, (3) solar wind velocity V_{SW}, (4) IMF B_Y, B_Z, and B_{IMF}, (5) Dst index, (6) Kp index, and (7) AE index. With forecasted driving parameter, the IMPTAM can predict the keV electron fluxes in the inner magnetosphere. The forecasted solar wind and IMF parameters are taken from the University of Warwick (https://warwick.ac.uk/fac/sci/physics/research/cfsa/people/bennett/swift-data/results3/). The forecasted geomagnetic indices are not provided by IRF-Lund, therefore, they are simply extrapolated during the forecasting period. The completely re-organized IMPTAM is now running online as IMPTAM real-time (GOES 15 comparison example, https://ssg.group.shef.ac.uk/progress2/html/imptam_results_ivg15.phtml) and IMPTAM forecast (GOES 15 example https://ssg.group.shef.ac.uk/progress2/html/imptam_fcast_g15_pdf.phtml). In real-time, IMPTAM outputs (a) the direct comparison with GOES 15 electron

fluxes for 40, 75 and 150 keV energies, (b) equatorial maps of electron fluxes for 1-10, 10-50, 50-100 and 100-200 keV energies, (c) energy-radial distance spectrograms for a current time moment at 0, 6, 12 and 18 MLT, (d) energy-time spectrograms along GOES 15, Galileo (MEO) and Van Allen Probes orbits. As forecast, IMPTAM outputs (i) energy-time spectrograms along GOES 15, Galileo (MEO) and Van Allen Probes orbits, and (ii) electron fluxes for 40, 75 and 150 keV energies along GOES 15 orbit, similar to what is observed. All outputs are available as API data for real-time (http://citrine.engin.umich.edu/imptam/api/result/realtime) and forecast (http://citrine.engin.umich.edu/imptam/api/result/forecast) and the plots are saved in the archive (http://citrine.engin.umich.edu/imptam/archive/realtime/ and http://citrine.engin.umich.edu/imptam/archive/forecast/).

10. References

Boyle, C. B., Reiff, P. H., and Hairston, M. R., Empirical polar cap potentials, *J. Geophys. Res.,* 102, 111-125, 1997.

Brautigam, D. H., and J. M. Albert, Radial diffusion analysis of outer radiation belt electrons during the October 9, 1990, magnetic storm, *J. Geophys. Res., 105*(A1), 291-310, 2000.

Carpenter, D. L., R. R. Anderson, ISEE/Whistler model of equatorial electron density in the magnetosphere, *J. Geophys. Res., 97*, 1097-1108, 1992.

Delcourt, D. C., Sauvaud, J.-A., Martin, Jr., R. F. and Moore, T. E.: On the nonadiabatic precipitation of ions from the near-earth plasma sheet, *J. Geophys. Res.*, 101, 17409-17418, 1996.

Dubyagin, S., N. Y. Ganushkina, I. Sillanpää, and A. Runov, Solar wind-driven variations of electron plasma sheet densities and temperatures beyond geostationary orbit during storm times, *J. Geophys. Res. Space Physics*, *121*, doi:10.1002/2016JA022947, 2016.

Fok, M.-C., et al., Global ENA IMAGE observations, *Space Sci. Rev., 109*, 77–103, 2003.

Ganushkina, N. Yu., T. I. Pulkkinen, T. Fritz, Role of substorm-associated impulsive electric fields in the ring current development during storms, Annales Geophysicae, Vol. 23, No. 2, 579-591, 2005.

Ganushkina N. Yu., O. Amariutei, Y. Y. Shpritz, and M. Liemohn, Transport of the plasma sheet electrons to the geostationary distances, *J. Geophys. Res.*, 118, doi:10.1029/2012JA017923, 2013.

Ganushkina N. Yu., M. Liemohn, O. Amariutei, and D. Pitchford, Low energy electrons (5-50 keV) in the inner magnetosphere, *J. Geophys. Res.*, 119, 246259, 549 doi:10.1002/2013JA019304, 2014.

Ganushkina, N. Y., O. A. Amariutei, D. Welling, and D. Heynderickx, Nowcast model for low-energy electrons in the inner magnetosphere, *Space Weather*, 13, doi:10.1002/2014SW001098, 2015.

Ganushkina, N. Yu., I. Sillanpaa, D. Welling, J. Haiducek, M. Liemohn, S. Dubyagin, J. V. Rodriguez, Validation of Inner Magnetosphere Particle Transport and Acceleration Model (IMPTAM) on the long-term measurements of keV electron fluxes at geostationary orbit by GOES MAGED instrument, submitted to *Space Weather*, under review, 2018.

Jordanova, V. K., J. Albert, and Y. Miyoshi, Relativistic electron precipitation by EMIC waves from self-consistent global simulations, *J. Geophys. Res.*, 113, A00A10, doi:10.1029/2008JA013239, 2008.

Li, X., D. N. Baker, M. Temerin, et al., Simulation of dispersionless injections and drift echoes of energetic electrons associated with substorms, *Geophys. Res. Lett.*, 25, 3763-3766, 1998.

Liemohn, M. W., and P. C. Brandt, Small-scale structure in the stormtime ring current, in *Inner Magnetosphere Interactions: New Perspectives From Imaging, Geophys. Monogr. Ser.*, vol. 159, edited by J. L. Burch, M. Schulz, and H. Spence, p. 167, AGU, Washington, D. C, 2005.

Orlova, K., and Y. Shprits, Model of lifetimes of the outer radiation belt electrons in a realistic magnetic field using realistic chorus wave parameters, J. Geophys. Res., 119, 770-780, doi:10.1002/2013JA019596, 2014.

Orlova, K., M. Spasojevic, and Y. Shprits, Activity-dependent global model of electron loss inside the plasmasphere, Geophys. Res. Lett., 41, doi:10.1002/2014GL060100, 2014.

Orlova, K., Y. Shprits, and M. Spasojevic, New global loss model of energetic and relativistic electrons based on Van Allen Probes measurements, J. Geophys. Res. Space Physics, 121, 1308-1314, doi:10.1002/2015JA021878, 2016.

Sarris, T. E, X. Li, N. Tsaggas, and N. Paschalidis, Modeling energetic particle injections in dynamic pulse fields with varying propagation speeds, *J. Geophys. Res.*, 107, 1033, doi: 10.1029/2001JA900166, 2002.

Schulz, M., and L. J. Lanzerotti, Particle Diffusion in the Radiation Belts, *Physics and Chemistry in Space*, vol. 7, 215 pp., Springer-Verlag, New York, 1974.

Sergeev, V. A. and Tsyganenko, N. A.: Energetic particle losses and trapping boundaries as deduced from calculations with a realistic magnetic field model, *Planet. Space Sci.*, 30, 999-1006, 1982.

Shprits Y. Y., and R. M. Thorne, Time dependent radial diffusion modeling of relativistic electrons with realistic loss rates, *Geophys. Res. Lett.*, 31, L08805, doi:10.1029/2004GL019591, 2004.

Sillanpää, I., Ganushkina, N. Y., Dubyagin, S., & Rodriguez, J. V., Electron fluxes at geostationary orbit from GOES MAGED data. *Space Weather*, *15*. https://doi.org/10.1002/2017SW001698, 2017.

Tsyganenko, N. A., Modeling the Earth's magnetospheric magnetic field confined within a realistic magnetopause, *J. Geophys. Res.*, 100, 5599-5612, 1995.